Effects of monopile installation on subsequent response in sand, Part II: lateral loading

Paper re-submitted to *Journal of Geotechnical and Geoenvironmental Engineering (ASCE)* on 22 Sep 2020 by:

Shengsheng Fan (corresponding author)

PhD candidate

Tel: +61 (0) 8 6488 6930

Email: shengsheng.fan@research.uwa.edu.au

Britta Bienen

Associate Professor

Tel: +61 (0) 8 6488 4246

Email: britta.bienen@uwa.edu.au

Mark F. Randolph

Professor

Tel: +61 (0) 8 6488 3075

Email: mark.randolph@uwa.edu.au

Centre for Offshore Foundation Systems
Oceans Graduate School
The University of Western Australia
35 Stirling Hwy
Crawley, Perth, WA 6009
Australia

No. of words: 5058 (excluding abstract, references and figures)

No. of tables: 5

No. of figures: 17

ABSTRACT

Monopiles under in-service conditions are subjected to lateral forces and resultant bending moments from the offshore environment. The subsequent lateral response following installation is significantly influenced by the ‘initial’ soil state post-installation, which is influenced by the pile installation process as demonstrated in previous numerical studies. To date, there are no technical guidelines established for consideration of installation effects on the design of laterally loaded monopiles. This paper is the second of a pair of companion papers that investigate the effect of different installation methods on subsequent response of monopiles under lateral loading. The paper focuses on the quantification of the effect of pile installation on the initial stiffness and lateral capacity. The numerical model is first validated against purpose-designed centrifuge tests. The analysis confirms that impact-driven piles have significantly higher initial stiffness and lateral capacity than jacked piles and wished-in-place piles. The effect of installation methods on the lateral response is also influenced by the initial soil density, driving distance, pile geometry, stress level, and load eccentricity. The study highlights the importance of considering the effects of the installation process on the subsequent lateral pile response.

Key words: monopile; installation effect; lateral response; sand; offshore engineering

INTRODUCTION

Monopiles with a diameter of 4-10 m and a length-to-diameter ratio of 3-6 are widely used as foundations for offshore wind turbines (OWTs), though to date limited guidance on evaluating the lateral response has been given in design guidelines such as DNVGL (2016). The conventional p-y method (API, 2011; Matlock, 1970; Reese et al., 1974) developed for long slender piles subjected to limited number of load cycles are not applicable for large-diameter monopiles used for OWTs (Abadie et al., 2019; Achmus et al., 2009, 2005; Bayton et al., 2018; Byrne et al., 2015; LeBlanc et al., 2010; Richards et al., 2019; Wu et al., 2019; Zdravković et al., 2015, among others). Significant improvements in the design methods have been achieved in the last few years through two well-known joint industry projects, PISA (Byrne et al., 2019) and REDWIN (Skau et al., 2018).

The PISA project proposed revised p-y curves by introducing additional rotational springs. These were validated against the results of 3D finite element modelling that had been calibrated against field test data. The REDWIN project represented the foundation response by a macro-element placed at the mudline. The relative merit of these two methods used in the design of monopiles in practice is discussed in Sturm and Andresen (2019). Both methods rely primarily on the finite element method (FEM) for the calibration of input parameters. However, all numerical simulations (Burd et al., 2020; Page et al., 2018; Taborda et al., 2019) are based on a wished-in-place assumption with soil profiles based on in-situ soil conditions from site investigations. The effect of the pile installation process on the in-situ soil conditions has not been taken into consideration.

Research including both physical modelling investigations and numerical investigations on the effect of pile installation on the subsequent response on monopile under lateral loading is limited, though design guidelines such as DNV (2014) acknowledge the importance of the effect of the installation process. A scaled centrifuge experimental study by Fan et al. (2019) reveals both the initial stiffness and bearing capacity are significantly affected by the installation methods. Numerical investigations by Heins and Grabe (2017) and Murphy et al. (2018) show the potential of using numerical methods to explore the effect of pile installation on the subsequent lateral response. However, since only very limited driving or jacking distance was simulated in these studies, the installation effect may not be fully captured.

OWTs are typically designed as ‘soft-stiff’ structures, with the target natural frequency lying between the rotational frequency (1P) and the blade passing frequency (3P) to avoid resonance and extend fatigue life. The narrow band of the target design frequency (f_0 in Figure 1) necessitates accurate prediction of the foundation stiffness. Natural frequencies of more than 400 offshore monopiles measured in the field have been reported to be larger than the design values (Achmus et al., 2019; Damgaard et al., 2014; Kallehave et al., 2015), which can mainly be attributed to underestimation of the foundation stiffness. A strict serviceability limit state (SLS) requirement on the permanent out of verticality of 0.5° is typically imposed for monopile foundations (DNVGL, 2016). The response of monopiles at this low operational displacement (strain) range is expected to be influenced significantly by the effects of installation, although the effects may reduce at very large displacements where significant plastic response of the soil is expected. Monopiles used for OWTs are typically installed into the seabed by impact driving. As shown in the first of the companion papers (Fan et al., 2020), the post-installation soil state, with indicators including stresses and void ratio, are significantly affected by the pile installation process. The effect of pile installation, therefore, needs to be taken into account for accurate prediction of the lateral response.

This is the second of the two companion papers, examining the effect of pile installation on the subsequent response under lateral loading. The numerical model developed was first validated against the test data from Fan et al. (2019). Two different installation methods including jacking and impact driving were considered and the response of a wished-in-place pile was also included for comparison. The numerical model developed allows quantification of the effect of pile installation on the initial stiffness and lateral capacity of monopiles under lateral loading. Further investigations of the effects of initial relative density, driving distance, pile geometry, stress level, and load eccentricity inform the conclusions drawn from this research.

DEVELOPMENT OF NUMERICAL MODEL

Pile lateral loading was modelled as a small strain finite element (SSFE) problem within the commercially available software Abaqus/Standard (Dassault Systèmes, 2014). Considering the symmetry of the problem, only half of the full model was simulated.

Numerical model

Figure 2 shows the mesh and boundary condition of a numerical model used. To facilitate comparison with measured test data, all relevant dimensions are taken from the centrifuge test by Fan et al. (2019), where a model monopile was tested at 100g. The model pile with a diameter of 50.0 mm and a wall thickness of 1.0 mm is made from a welded pipe using V2A-steel (material number 1.4301) according to European standard DIN EN 10088-3 (DIN, 2014). The external epoxy coating used to protect the strain gauges has a wall thickness of around 1.1 mm. The corresponding prototype monopile with an overall diameter (D_{pile}) of 5.22 m and a wall thickness of 0.21 m was simulated. As the pile flexural stiffness may not be neglected when investigating the lateral response, the pile steel and epoxy coating were modelled as a linear elastic material, with material properties summarized in Table 1. The detail of the transition from the steel to epoxy is shown in Figure 2. A second pile geometry of an 8 m diameter pile with a constant 0.1 m wall thickness was also included.

The load eccentricity-to-diameter ratio (I_e/D_{pile} = 3.8) and embedment length-to-diameter ratio (L_e/D_{pile} = 3.1) were chosen to match the physical test conditions. The lateral loading (pile was pushed from right to left, see Figure 2) was applied at a reference point defined at a distance of I_e above the soil surface, resulting in a horizontal load of H and a moment of $M = H \cdot I_e$ at the pile head. A constant load eccentricity of $3.8D_{pile}$ was used throughout. The static monotonic lateral loading can be applied through load-controlled method or displacement-controlled methods with indistinguishable results as no pore fluid effects were modelled.

The radius and depth of the soil domain are identical to those used in the pile installation model described in the first of the companion papers (Fan et al., 2020), with a width of $10.8D_{pile}$ and a depth of $7.6D_{pile}$. The soil surface post installation (Fan et al. 2020) was approximated by a spline, which was revolved for the 3D lateral loading model. The side of the soil domain is restrained from any lateral displacement and the base of the soil domain is restrained from any vertical displacement. The mesh used in this study is similar to that used in the pile installation analysis. A convergence study for a wished-in-place pile confirmed the mesh used is sufficient for the accuracy of the analysis.

Soil characteristics and constitutive model

The properties of very fine UWA silica sand are given in Table 1 of the first of the companion papers (Fan et al., 2020). The sand was modelled using a rate-independent hypoplastic constitutive law by (Kolymbas, 1991, 1985) in the form proposed by von Wolffersdorff, (1996) with the enhancement of intergranular strains by Niemunis and Herle, (1997). The user subroutine of the UMAT implementation for Abaqus/Standard by Gudehus et al. (2008), as available on soilmodels.com, was used. The hypoplastic constitutive model parameters are given in Table 2 of Fan et al. (2020).

Initial soil state and mapping procedure

To capture the effect of pile installation, the post-installation soil state needs to be taken into account in the lateral loading model. The results (stress and state-dependent variables) obtained from the pile installation model (Fan et al. 2020) were mapped to the lateral loading as initial soil conditions following the methodology outlined by Heins and Grabe (2017). Only one-quarter of the full model was simulated during the installation phase, while half of the full model was simulated during the lateral loading phase. The installation results were therefore mirrored first before performing a 3D-interpolation using a code implemented in Matlab. The procedure of mapping the soil state from the pile installation analysis (Fan et al., 2020) to the lateral loading model is shown in Figure 3. Figure 4 shows an example of mapping results of a) void ratio, b) horizontal stress from the installation analysis of pile jacking (LHS) to the SSFE analysis for the pile lateral loading model (RHS). An equilibrium step was required following the mapping procedure to establish the post-installation 'initial' soil state.

Contact properties

A surface-to-surface (master-slave type) contact was used to describe the interface between the pile and the soil. The contact properties were kept the same as the properties used in the pile installation analysis (Fan et al., 2020). The pile internal wall and the pile tip were modelled as frictionless. A roughness of $\tan\delta/\tan\phi_c = 0.5$ was assumed for the pile external wall, where δ is the interface friction angle between the pile and sand, ϕ is the critical friction angle of the sand.

VALIDATION OF THE NUMERICAL MODEL

The accuracy of the numerical model was validated by comparison of numerical analysis results and the centrifuge experimental test data (Fan et al., 2019). The purpose-designed apparatus used in the test allows both in-flight installation using different installation methods and in-flight lateral loading (post-installation) without stopping the centrifuge which is important to retain the post-installation soil state. The test was conducted in a dry medium dense sand with an initial relative density of 38%. Details regarding the centrifuge tests are given in Fan et al. (2019).

Numerical simulation of monotonic push-over of a monopile following either pile jacking or impact driving was simulated to replicate the test conditions. A summary of the analyses conducted is given in Table 2, which includes a wished-in-place pile for comparison. Only dimensionless quantities are given in the following discussion unless noted otherwise. The lateral displacement is normalised by the pile overall diameter D_{pile}. The lateral force and bending moment are normalised by γD_{pile}^3 and γD_{pile}^4 respectively, where γ is the unit weight of the sand. The stiffness H/y_0, where y_0 is the pile head displacement at the original soil surface, is normalised by γD_{pile}^2.

Load-displacement response

Figure 5 shows the comparison of the normalised load-displacement curves from numerical analysis and the centrifuge test. In published numerical and experimental studies (e.g. Byrne et al., 2019; Klinkvort and Hededal, 2014), piles are generally pushed to a lateral displacement of 10% of the pile diameter at the pile head, which is widely accepted as an ultimate limit state (ULS) design limit. However, in general long before the ultimate capacity is mobilised, the pile deformations exceed the SLS design limit. The SLS design criterion (DNV, 2014; DNVGL, 2016) limits the total tilt rotation at the mudline to 0.5°. For the current pile and soil conditions, a normalised pile head displacement of 0.04 corresponds to a tilt rotation at the mudline of 0.98° and 0.88° respectively for driven piles and jacked piles. This is almost twice the SLS design limit. Therefore, only the response up to a pile head displacement of $0.04D_{pile}$ is presented here as this covers the entire operational range of monopiles.

Overall, the normalised load-displacement curves from the numerical analysis match well with those deduced from centrifuge tests for both jacked piles and driven piles. The impact-driven piles exhibit stiffer load-displacement response than jacked piles, while the wished-in-place piles exhibit the softest load-displacement response which is similar to the test data of piles jacked at 1g. The post-installation soil state is well captured by the numerical model, in particular, the initial stiffness is appropriately reflected. The impact-driven experimental results appear overly stiff initially due to challenges in accurately measuring extremely small displacements and extrapolating these from the point of measurement down to the pile head. The numerical analyses overestimate the lateral capacity of jacked piles mobilised at $0.02D_{pile}$ and $0.04D_{pile}$ pile head displacement by 8% and 24%, respectively. The numerical analyses overestimate the lateral capacity of driven piles mobilised at $0.02D_{pile}$ and $0.04D_{pile}$ pile head displacement by 18% and 36%, respectively.

Neglecting the effects of pile installation is likely to result in inaccurate prediction of lateral response, and hence the natural frequency of the overall OWT. At large displacements, the numerical results overestimate the lateral capacity, as the stiffness declines more slowly than in the physical test. A similar overestimation of lateral capacity at larger displacement (> 20 mm, namely 0.04 pile diameter in this study) was also suggested by Murphy et al. (2018) where the trend of numerical analysis results based on a non-linear stress-dependent Hardening Soil model started to exceed field test data, although the response at smaller displacement (< 20 mm) matched well with the field test data.

The ‘initial’ soil state for driven piles was based on results of pile driving analysis with a higher impact driving force than the actual test condition in consideration of the computational cost. The analysis result is still highly consistent with the test data as long as the entire driving process is modelled.

Secant stiffness

Figure 6 compares the normalised secant stiffness obtained from numerical analysis and centrifuge test results. A continuous secant stiffness profile can be extracted from the numerical analysis results. The experimental secant stiffness at the small displacement range (< 0.001 or 52.2 μm for a model pile with a diameter of 52.2 mm) is very difficult to obtain due to the challenges in accurately measuring extremely small displacements. Overall, the normalised secant stiffness reported by numerical analyses matches reasonably well with the centrifuge test data. The numerical analyses underestimate the secant stiffness mobilised at $0.002D_{pile}$ pile head displacement by 9% and 23% for jacked piles and driven piles, respectively. Wished-in-place piles have slightly higher initial stiffness than jacked piles at the very small displacement range (< 0.0003) in Figure 6.

This is mainly attributed to the dilation as a result of the installation process observed in the pile/soil interface for jacked piles. The stiffness of wished-in-place piles is very close to piles jacked at 1g in centrifuge tests. Numerical results based on wished-in-place piles and centrifuge experimental results based on 1g jacking installation lead to underestimation of the lateral resistance.

Pile deflection, shear force and bending moment distribution

Figure 7 shows the pile deflection, shear force and bending moment profiles along the pile length from numerical analyses for two load levels ($H/\gamma D_{pile}^3$ = 0.9 and 2.8), where $z > 0$ denotes the section above the mudline and $z \leq 0$ denotes the embedded pile section. Figure 7a indicates the rotation point is located at around 77% and 85% of embedded pile length for impact-driven piles and jacked piles respectively (pile was pushed from RHS to LHS). The corresponding displacement and rotation at pile head at these two load levels are summarized in Table 3. Figure 7c shows excellent agreement between the measured bending moment and moment reported by the numerical simulation (especially at the small load level of $H/\gamma D_{pile}^3$ = 0.9). The maximum difference between the moment measured in the test and the moment reported from numerical analyses at the large load level of $H/\gamma D_{pile}^3$ = 2.8 is less than 7% for both jacked and driven piles. Jacked piles exhibit much larger displacement (Figure 6a) than impact-driven piles at the same load level, although the differences in the shear force (Figure 6b) and bending moment profiles (Figure 7c) are relatively minor. The greater stiffness of the impact-driven piles arises from the effects of impact driving, as discussed in the following section.

VALIDATION AND DISCUSSION OF SOIL STATE CHANGES DUE TO PILE INSTALLATION

The numerical results show impact-driven piles have significantly higher initial stiffness and lateral capacity than jacked piles. This finding is consistent with the centrifuge test results reported by Fan et al. (2019), and arises from the post-installation soil conditions, in particular the distributions of horizontal stress and void ratio, following different installation methods. The contours of void ratio and horizontal stress following jacking and impact driving are given respectively in Figure 13a and Figure 14a of Fan et al. (2020). The contours of void ratio and horizontal stress when the pile head is pushed to 0.04 lateral displacement are given in Figure 8. Figure 9 shows the changes in void ratio and horizontal stress from post-installation ('initial' state) to 0.04 mudline displacement. The pattern of changes in the lateral stress and void ratio is similar for all installation methods, but the extent and magnitude of the changes on the passive side depend significantly on the installation method. The impact-driven piles have the highest increase in the horizontal stress on the passive side, while the decrease in the void ratio is smaller especially in the area next to the pile/soil interface as soil has been densified to a greater extent due to the driving process. The wished-in-place piles have the lowest change in horizontal stress. The subsequent lateral response reflects these different installation-induced soil states.

Figure 10 shows the p-y curves generated from the numerical analyses results at four different soil depths. The p-y curves were extracted from the numerical analysis results, with p obtained by double-differentiating the bending moment along the pile length and y directly from the pile lateral displacement. The p-y curves are significantly affected by the method of installation. Soil pressures mobilised for impact-driven piles at a given displacement and depth are significantly higher than for jacked or wished-in-place piles, especially at shallow depth (z = -0.5, 1.0 and 1.5D_{pile}) where the soil has been significantly densified (Fan et al., 2020), and also near the pile toe (z = -2.8D_{pile}). This is also consistent with the observation of a significantly higher increase in the horizontal stress as reported in Figure 8 when the impact-driven pile is loaded laterally.

Most of the published numerical studies do not account for installation effects due to the limitation of numerical tools and consideration of the extremely high computation costs. As shown here, both the initial stiffness and lateral capacity are significantly underestimated if the installation-induced void ratio and horizontal stress are not accounted for. An underestimation of the stiffness will lead to underestimation of the natural frequency. This may be one of the reasons why the design frequency of hundreds of offshore wind turbines is actually lower than the measured frequency (Achmus et al., 2019; Damgaard et al., 2014; Kallehave et al., 2015).

PARAMETRIC STUDY

Further exploration of factors that may influence the effect of installation methods on the subsequent lateral response were conducted using the validated numerical model. Factors including initial relative density, driving distance, pile geometry, stress level, and load eccentricity were examined.

Effect of initial relative density

The normalised load-displacement curves and secant stiffness for three different initial relative densities (D_R =38, 60 and 88%) are given in Figure 11 and Figure 12 respectively. All analyses were conducted using the test pile dimensions (5.22 m pile), embedment length-to-diameter ratio (L_e/D_{pile} = 3.1) and load eccentricity-to-diameter ratio (I_e/D_{pile} = 3.8). As expected, both the initial stiffness and lateral capacity increase with the initial relative density, regardless of installation method. In terms of the effect of installation method, the impact-driven piles have significantly higher initial stiffness and lateral capacity than jacked piles and wished-in-place piles, consistently for sand of different initial relative densities. The most remarkable difference in the response between the jacked piles and impact-driven piles was found for dense sand (D_R =88%), while wished-in-place piles exhibited the softest response. Dilation resulting from pile jacking, and consequent increases in void ratio near the pile, leads to reduced stiffness at the small displacement range. An increase in the void ratio in the area next to the pile external wall/soil interface is observed for sand of different relative densities following jacking (as shown in Figure 7a, 9a, and 11a of Fan et al., 2020). At larger displacement range (>0.001), the jacked piles have a higher secant stiffness and lateral capacity than wished-in-place piles due to the combined effect of the increase in horizontal stress and decrease in void ratio for sand with initial relative densities of 38% and 60%. For the dense sand case (D_R = 88%), the jacked piles also have a stiffer lateral response than wished-in-place piles due to the increase in the horizontal stress during installation, even though significant dilation occurs (see Figure 11a, Figure 12a of Fan et al., 2020). Details of the changes in void ratio and horizontal stress in the surrounding soil following pile installation can be seen in Figure 7-12 of Fan et al., 2020.

The initial stiffness defined as secant stiffness at 0-0.001 mudline displacement after McAdam et al. (2019) is summarized in Table 4. The secant stiffness defined at 0-0.04 mudline displacement is summarized in Table 5. The increase of the initial stiffness and secant stiffness due to different pile installation methods is also given.

Effect of driving distance

From a practical perspective, significant computational cost can be saved if the required driving distance to be simulated can be reduced, yet its effect on the lateral response needs to be investigated. Figure 13 (blue lines) shows the results of analyses where the simulated driving distance was varied, maintaining the same total embedment length. The pre-jacked distance was varied accordingly. The results for wished-in-place piles and jacked pile (black lines) are also given for comparison. The results show both the initial stiffness and lateral capacity increase as the simulated driving distance increases. The initial stiffness and lateral capacity for 1.3D_{pile} and 2.2D_{pile} driving cases are very similar. The initial stiffness reported for 0.6D_{pile} driving case is still comparable, but the lateral capacity is significantly underestimated as a low driving distance predominantly changes soil state around the pile toe, with little effect along the embedded length of the pile. A sufficient driving distance is required to capture the changes of the soil state due to impact driving in the region closer to the soil surface that is more significant for the lateral response. Significant computational cost can be saved by pre-jacking the pile while retaining the accuracy of initial stiffness, while the lateral capacity at larger displacement is underestimated.

An additional study was performed by wishing the pile in place by an embedment length of $2.1D_{pile}$ and only modelling the last $1.0D_{pile}$ driving. Both the initial stiffness and lateral capacity are underestimated as shown in Figure 13 (red line), lower than any of the pre-jacked cases. This is most likely due to the reduced volume of penetration resulting from the wished-in-place technique. In addition to the driving distance, the volume of the body penetrating into soil is also of significant importance to the post-installation conditions and hence the subsequent lateral response.

Effect of pile geometry and stress level

All discussions in the section above are based on the pile dimensions (5.22 m pile) modelled experimentally. Monopiles with diameters exceeding 8 m and a wall thickness of around 0.1 m are currently being used in the offshore wind industry, e.g. Rentel wind farm in Belgium (Degraer et al., 2018). Analyses considering a monopile with a diameter of 8 m and a wall thickness of 0.1 m were conducted to investigate the influence of stress level and pile geometry. The same load eccentricity-to-diameter ratio and embedment length-to-diameter ratio were maintained.

The effect of stress level was first examined by comparing the response of wished-in-place piles, where the installation effect was ignored. Figure 14 compares the response of two piles in sand of three different initial relative densities. In general, the smaller pile (5.22 m pile) has a higher normalised initial stiffness and lateral capacity than the large (8 m) diameter pile for all relative densities considered. The influence of installation method on the horizontal stresses was also examined. Figure 15 compares the response of two piles installed using different methods in sand with an initial relative density of 38%. The results for wished-in-place piles are also included for comparison. The observation is that smaller piles exhibit a stiffer response than the larger diameter pile following either jacking or impact driving. This is consistent with the observation that the lateral response becomes softer as the stress level increases, as reported by Klinkvort (2013) from centrifuge tests where the model piles were jacked at 1g.

Only the last ~1.2-1.3D_{pile} impact driving distance was simulated and piles were pre-jacked to ~1.8-1.9D_{pile} before impact driving was initiated considering the high computational cost as explained in the companion paper (Fan et al., 2020).

Figure 15 also shows the magnitude of differences in both initial stiffness and lateral capacity due to different installation methods are more remarkable for the tested small pile. In contrast, both the initial stiffness and lateral capacity of the jacked and impact-driven 8 m diameter piles are almost identical but larger than for the wished-in-place piles. This may be attributed to the difference in the effective area of the piles. The diameter-to-wall thickness ratios (D/t) of the 5.22 m and 8 m piles are 25 and 80, respectively. The effective area ratios ($A_r = 1 - (D_i/D_o)^2$) are 0.15 and 0.05 respectively, where D_i is the pile internal diameter of pile, D_o is the pile external diameter. The pile installation process and resulting post-installation soil state is affected significantly by the effective area ratio of piles (Lehane et al., 2005). As shown in Figure 18 of Fan et al. (2020), less marked changes in soil states due to pile driving are reported for the 8 m pile than those reported for the 5.22 m pile due to the combined effect of the reduced driving distance and reduced effective area. The effect of pile installation on the subsequent lateral response is therefore more evident for piles with smaller D/t ratio or large effective area ratio.

The responses of 8 m diameter piles in sand with an initial relative density of 60% and 88% are shown in Figure 16. The most significant difference between the response of jacked piles and driven piles is also reported in dense sand (D_R = 88%), similar to the results for the 5.22 m pile. Overall, the impact-driven piles generally have a higher lateral capacity and secant stiffness at displacements less than ~0.004 and at displacements larger than 0.04 for all relative densities, while the jacked piles have higher lateral resistance at intermediate displacements, varying according to the soil density.

Effect of load eccentricity

Analyses considering five different load eccentricities were conducted to illustrate the effect of load eccentricity. As an example, sand with an initial relative density of 60% and two different installation methods were considered. The embedment length-to-diameter ratio was kept as 3.1. The lateral capacity and the secant stiffness of piles loaded at five different load eccentricities (I_e/D_{pile} = 2.0, 3.8, 6.0, 8.0 and 10.0) for jacked and driven large diameter piles are shown in Figure 17a and Figure 17b respectively. As expected, both the initial stiffness and lateral capacity increase significantly as the load eccentricity and hence the moment component decreases, as also reported in the centrifuge experimental study by Klinkvort and Hededal (2014). Figure 17b shows that there are large differences in the initial stiffness between the jacked and driven piles for small load eccentricities. However, the magnitude of the difference in the initial stiffness decreases significantly as the load eccentricity increases.

CONCLUSIONS

This paper has discussed findings from a numerical investigation of the effect of different pile installation methods on the subsequent lateral response. A systematic study of the effects of soil initial relative density, pile driving distance, pile geometry, stress level, and load eccentricity was conducted. The following key conclusions are drawn based on the results.

- The initial stiffness and lateral capacity over the displacement range within typical serviceability criteria are significantly affected by the post-installation soil state, which in turn is affected by the pile installation method. Impact-driven piles can have significantly higher initial stiffness and lateral capacity than jacked piles, regardless of the initial soil relative density but depending on the D/t ratio. Wished-in-place conditions, as commonly adopted in practice, will lead to an underestimation of both initial stiffness and lateral capacity, and consequently, an underestimation of the natural frequency of OWTs.
- For a pile with a diameter of 5.22 m and a wall thickness of 0.21 m (D/t = 25), considering an embedded length of 3.1 pile diameters and a load eccentricity of 3.8 pile diameters, the initial stiffnesses following impact-driven and jacked installation are (on average for different relative densities) respectively 47% and 10% higher than following wished-in-place conditions. The lateral capacity of impact-driven and jacked piles at a mudline displacement of $0.04D_{pile}$ (rotation of around 1°) are 76% and 19% higher than for wished-in-place piles for this example. The effect is diminished for larger piles with larger D/t ratios.

- The results confirmed the effect of the ambient stress level on the pile lateral response. A larger pile (higher ambient stress levels) always gives a softer response (once normalized by the pile size), and this holds for different initial relative densities and different installation methods.
- The differences in the initial stiffness and lateral capacity following different installation methods are affected by pile geometry. The difference in the lateral response is more significant for piles with a smaller D/t ratio or large effective area. Impact driving leads to a more substantial increase in the initial stiffness and lateral capacity for piles with a smaller D/t ratio or larger effective area.
- The decrease in initial stiffness and lateral capacity with increasing load eccentricity has been documented. The magnitude of the difference in the initial stiffness of jacked piles and driven piles decreases significantly as the load eccentricity increases.
- To capture the effects of impact-driven pile installation along the shaft as well as around the pile toe, which will be reflected in the initial stiffness and pile capacity, sufficient impact driving needs to be simulated over a sufficient penetration distance. For driven piles, significant computational cost can be saved by pre-jacking the pile without losing accuracy with respect to the initial stiffness. Although the assumption of wished-in-place conditions can save considerable computational costs, this will lead to underestimation of both initial stiffness and lateral capacity.

DATA AVAILABILITY STATEMENT

The measurement data and model output are available from the corresponding author by request.

ACKNOWLEDGEMENTS

This work forms part of the activities of the Centre for Offshore Foundation Systems (COFS), which is currently supported as a Centre of Excellence by the Lloyd’s Register Foundation and through the Fugro Chair in Geotechnics and the Shell EMI Chair in Offshore Engineering. Lloyd’s Register Foundation helps to protect life and property by supporting engineering-related education, public engagement and the application of research. This support is gratefully acknowledged.

NOTATIONS

D_{pile}	[m]	Overall pile diameter (including epoxy)
D_R	[-]	Relative density of sand
e	[-]	Void ratio
f_0	[-]	Design frequency
H	[N]	Lateral force/load
L_e	[m]	Embedded pile length
I_e	[m]	Load eccentricity
M	[Nm]	Bending moment
S	[N]	Shear force
y_0	[m]	Lateral displacement at mudline/pile head
y	[m]	Lateral displacement
z	[m]	Pile depth
δ	[º]	Interface friction angle between pile and sand
Δe	[-]	Changes in void ratio
$\Delta\sigma_{11}$	[kPa]	Changes in horizontal stress
φ	[º]	Critical friction angle of sand
σ_{11}	[kPa]	Horizontal stress
θ_0	[º]	Rotation at mudline/pile head
γ	[kN/m^3]	Sample dry density

REFERENCES

Abadie, C.N., Byrne, B.W., Houlsby, G.T., 2019. Rigid pile response to cyclic lateral loading: Laboratory tests. *Geotechnique*. 69, 863–876. https://doi.org/10.1680/jgeot.16.P.325

ABAQUS user's manual, version 6.14, 2014. . Dassault Systèmes Simulia Corp, Providence, RI, USA.

Achmus, M., Abdel-Rahman, K., Peralta, P., 2005. On the design of monopile foundations with respect to static and quasi-static cyclic loading, in: Copenhagen Offshore Wind. pp. 1–9.

Achmus, M., Kuo, Y.-S., Abdel-Rahman, K., 2009. Behavior of monopile foundations under cyclic lateral load. *Computers and Geotechnics*. 36, 725–735. https://doi.org/10.1016/j.compgeo.2008.12.003

Achmus, M., Thieken, K., Saathoff, J.-E., Terceros, M., Albiker, J., 2019. Un-and reloading stiffness of monopile foundations in sand. *Applied Ocean Research*. 84, 62–73. https://doi.org/10.1016/j.apor.2019.01.001

API, 2011. 2GEO Geotechnical and foundation design considerations. Washington, DC, USA: American Petroleum Institute.

Bayton, S.M., Black, J.A., Klinkvort, R.T., 2018. Centrifuge modelling of long term cyclic lateral loading on monopiles, in: Physical Modelling in Geotechnics. pp. 689–694. https://doi.org/10.1201/9780429438660-103

Burd, H.J., Taborda, D.M.G., Zdravković, L., Abadie, C.N., Byrne, B.W., Houlsby, G.T., Gavin, K.G., Igoe, D.J.P., Jardine, R.J., Martin, C.M., others, 2020. PISA design model for monopiles for offshore wind turbines: application to a marine sand. *Géotechnique*. 1–19. https://doi.org/10.1680/jgeot.18.P.277

Byrne, B., McAdam, R., Burd, H., Houlsby, G., Martin, C., C, L., Taborda, D., Potts, D., Jardine, R., Sideri, M., Schroeder, F., Gavin, K., Doherty, P., Igoe, D., Wood, A., Kallehave, D., Gretlund, J., 2015. New design methods for large diameter piles under lateral loading for offshore wind applications, in: Frontiers in Offshore Geotechnics III. Taylor & Francis, London, pp. 705–710. https://doi.org/10.1201/b18442-96

Byrne, B.W., Burd, H.J., Zdravkovic, L., Abadie, C.N., Houlsby, G.T., Jardine, R.J., Martin, C.M., McAdam, R.A., Pacheco Andrade, M., Pedro, A.M.G., others, 2019. PISA design methods for offshore wind turbine monopiles, in: Offshore Technology Conference. Offshore Technology Conference. https://doi.org/10.4043/29373-MS

Damgaard, M., Bayat, M., Andersen, L. V., Ibsen, L.B., 2014. Assessment of the dynamic behaviour of saturated soil subjected to cyclic loading from offshore monopile wind turbine foundations. *Computers and Geotechnics*. 61, 116–126. https://doi.org/10.1016/j.compgeo.2014.05.008

Degraer, S., Brabant, R., Rumes, B., Vigin, L., 2018. Environmental Impacts of Offshore Wind Farms in the Belgian Part of the North Sea: Assessing and Managing Effect Spheres of Influence, Royal Belgian Institute of Natural Sciences, OD Natural Environment, Marine Ecology and Management.

DIN EN 10088-3, 2014. Stainless steels – Part 3: technical delivery conditions for semi-finished products, bars, rods, wire, sections and bright products of corrosion resisting steels for general purposes. Berlin, Germany.

DNV, 2014. Offshore standard DNV-OS-J101: Design of offshore wind turbine structures. Hoevik, Norway: Det Norsok Veritas.

DNVGL, 2016. DNVGL-ST-0126: Support structures for wind turbines, DNVGL AS. Hoevik, Norway: Det Norsok Veritas and Germanischer Lloyd.

Fan, S., Bienen, B., Randolph, M.F., 2020. Effects of monopile installation on subsequent lateral response in sand, Part I: pile installation. *Journal of Geotechnical and Geoenvironmental Engineering, ASCE.*

Fan, S., Bienen, B., Randolph, M.F., 2019. Centrifuge study on effect of installation method on lateral response of monopiles in sand. *International Journal of Physical Modelling in Geotechnics*. 1–13. https://doi.org/10.1680/jphmg.19.00013

Gudehus, G., Amorosi, A., Gens, A., Herle, I., Kolymbas, D., Mašín, D., Wood, D.M., Niemunis, A., Nova, R., Pastor, M., Tamagnini, C., Viggiani, G., 2008. The soilmodels.info project. *International Journal for Numerical and Analytical Methods in Geomechanics*. 32, 1571–1572. https://doi.org/10.1002/nag.675

Heins, E., Grabe, J., 2017. Class-A-prediction of lateral pile deformation with respect to vibratory and impact pile driving. *Computers and Geotechnics*. 86, 108–119. https://doi.org/10.1016/j.compgeo.2017.01.007

Kallehave, D., Byrne, B.W., LeBlanc Thilsted, C., Mikkelsen, K.K., 2015. Optimization of monopiles for offshore wind turbines. *Philosophical Transactions of the Royal Society A: Mathematical, Physical and Engineering Sciences*. 373.

https://doi.org/10.1098/rsta.2014.0100

Klinkvort, R.T., 2013. Centrifuge modelling of drained lateral pile - soil response: Application for offshore wind turbine support structures. Doctoral dissertation, Technical University of Denmark, Lyngby, Denmark.

Klinkvort, R.T., Hededal, O., 2014. Effect of load eccentricity and stress level on monopile support for offshore wind turbines. *Canadian Geotechnical Journal*. 51, 966–974. https://doi.org/10.1139/cgj-2013-0475

LeBlanc, C., Houlsby, G.T., Byrne, B.W., 2010. Response of stiff piles in sand to long-term cyclic lateral loading. *Géotechnique*. 60, 79–90. https://doi.org/https://doi.org/10.1680/geot.7.00196

Lehane, B.M., Schneider, J.A., Xu, X., 2005. The UWA-05 method for prediction of axial capacity of driven piles in sand, in: GOURVENEC, S.M., Cassidy, M.J. (Eds.), In Frontiers in Offshore Geotechnics: Proceedings of the 1st International Symposium on Frontiers in Offshore Geotechnics (ISFOG2005). Taylor and Francis, London, UK, Perth, pp. 683–689.

Matlock, H., 1970. Correlation for design of laterally loaded piles in soft clay, in: Offshore Technology Conference. Houston, Texas. https://doi.org/10.4043/1204-MS

McAdam, R.A., Byrne, B.W., Houlsby, G.T., Beuckelaers, W.J.A.P., Burd, H.J., Gavin, K., Igoe, D., Jardine, R.J., Martin, C.M., Muir Wood, A., Potts, D.M., Skov Gretlund, J., Taborda, D.M.G., Zdravković, L., 2019. Monotonic laterally loaded pile testing in a dense marine sand at Dunkirk. *Géotechnique*. 1–34.

https://doi.org/10.1680/jgeot.18.pisa.004

Murphy, G., Igoe, D., Doherty, P., Gavin, K., 2018. 3D FEM approach for laterally loaded monopile design. *Computers and Geotechnics*. 100, 76–83. https://doi.org/10.1016/j.compgeo.2018.03.013

Niemunis, A., Herle, I., 1997. Hypoplastic model for cohesionless soils with elastic strain range. *Mechanics of Cohesive-frictional Materials*. 2, 279–299.

Page, A.M., Grimstad, G., Eiksund, G.R., Jostad, H.P., 2018. A macro-element pile foundation model for integrated analyses of monopile-based offshore wind turbines. *Ocean Engineering*. 167, 23–35. https://doi.org/10.1016/j.oceaneng.2018.08.019

Reese, L.C., Cox, W.R., Koop, F.D., 1974. Analysis of laterally loaded piles in sand, in: Offshore Technology Conference. Houston, Texas. https://doi.org/doi.org/10.4043/2080-MS

Richards, I.A., Byrne, B.W., Houlsby, G.T., 2019. Monopile rotation under complex cyclic lateral loading in sand. *Géotechnique*. 1–15. https://doi.org/10.1680/jgeot.18.p.302

Skau, K.S., Page, A.M., Kaynia, A.M., Løvholt, F., Norén-Cosgriff, K., Sturm, H., Andersen, H.S., Nygard, T.A., Jostad, H.P., Eiksund, G., Havmøller, O., Strøm, P., Eichler, D., 2018. REDWIN - REDucing cost in offshore WINd by integrated structural and geotechnical design. *Journal of Physics: Conference Series*. 1104. https://doi.org/10.1088/1742-6596/1104/1/012029

Sturm, H., Andresen, L., 2019. On the Use of the Finite Element Method for the Design of Offshore Wind Turbine Foundations, in: Wu W. (Eds) Desiderata Geotechnica. Springer Series in Geomechanics and Geoengineering. Springer, Cham, pp. 193–204. https://doi.org/10.1007/978-3-030-14987-1_23

Taborda, D.M.G., Zdravković, L., Potts, D.M., Burd, H.J., Byrne, B.W., Gavin, K.G., Houlsby, G.T., Jardine, R.J., Liu, T., Martin, C.M., others, 2019. Finite-element modelling of laterally loaded piles in a dense marine sand at Dunkirk. *Géotechnique*. 1–16. https://doi.org/10.1680/jgeot.18.PISA.006

von Wolffersdorff, V., 1996. Mechanics of Cohesive-Frictional Materials hypoplastic model. *Mechanics of Cohesive-frictional Materials*. 1, 251–271.

Wu, X., Hu, Y., Li, Y., Yang, J., Duan, L., Wang, T., Adcock, T., Jiang, Z., Gao, Z., Lin, Z., Borthwick, A., Liao, S., 2019. Foundations of offshore wind turbines: A review. *Renewable and Sustainable Energy Reviews*. 379–393. https://doi.org/10.1016/j.rser.2019.01.012

Zdravković, L., Taborda, D., Potts, D., Jardine, R., Sideri, M., Schroeder, F., Byrne, B., McAdam, R., Burd, H., Houlsby, G., Martin, C., Gavin, K., Doherty, P., Igoe, D., Wood, A., Kallehave, D., Gretlund, J., 2015. Numerical modelling of large diameter piles under lateral loading for offshore wind applications, in: Frontiers in Offshore Geotechnics III. pp. 759–764. https://doi.org/10.1201/b18442-105

TABLES

Table 1 Pile material properties

Material	Young's modulus [GPa]	Poisson's ratio [-]
Pile - steel	200	0.27
Epoxy coating	2	0.33

Table 2 Summary of numerical analysis for validation, D_R = 38%

Case	D_{pile} [m]	WT [m]	L_e/D_{pile}	Pile installation method	Lateral loading type
1				Wished-in-place	
2	5.22	0.21	3.1	Jacking	Monotonic push over
3				Impact driving	

Table 3 Mudline displacement and mudline rotation at two load levels

Installation method	Load level $H/\gamma D^3 = 0.9$		Load level $H/\gamma D^3 = 2.8$	
	y_0 [-]	θ_0 [°]	y_0 [-]	θ_0 [°]
Impact driving	0.002	0.07	0.023	0.61
Jacking	0.004 (109%)	0.11 (60%)	0.040 (79%)	0.97 (59%)

Notes:

1) y_0 denotes the mudline displacement, θ_0 denotes the mudline rotation
2) The values given in parentheses denote the difference in percentage compared with driven piles.

Table 4 Initial stiffness (secant stiffness at 0-0.001 mudline displacement)

Installation method	Initial stiffness		
	D_R = 38%	D_R = 60%	D_R = 88%
WIP	358.6	387.3	704.3
Jacking	409.6 (14.2%)	404.8 (4.5%)	775.6 (10.1%)
Impact driving	550.9 (53.6%)	562.3 (45.2%)	1004.4 (42.6%)

Note:

1) The values given in parentheses denote the increase of initial stiffness compared with wished-in-place piles.

Table 5 Secant stiffness (secant stiffness at 0-0.04 mudline displacement)

Installation method	Secant stiffness		
	$D_R = 38\%$	$D_R = 60\%$	$D_R = 88\%$
WIP	55.2	63.8	149.5
Jacking	68.8 (24.8%)	75.3 (18.0%)	169.8 (13.8%)
Impact driving	90.8 (64.7%)	102.7 (61.0%)	300.3 (100.9%)

Note:

1) The values given in parentheses denote the increase of lateral capacity at 0.04 mudline displacement compared with wished-in-place piles.

Figure 1 Excitation ranges of OWTs in the frequency domain (after Kallehave et al., 2015)

Figure 2 Lateral loading model (mesh, boundary conditions)

Figure 3 Mapping procedure from pile installation model to lateral loading model

Figure 4 Soil state following jacked pile installation (D_R = 38%), (a) void ratio (b) horizontal stress (kPa). Results from pile installation (LHS, Fan et al. 2020) and mapped to pile lateral loading model (RHS)

Figure 5 Comparison of normalised load-displacement curves between current numerical study and centrifuge test data, D_R = 38%

Figure 6 Comparison of normalised secant stiffness between current numerical study and centrifuge test, D_R = 38%

Figure 7 Deflection, shear force, and bending moment profiles along the entire pile length

Figure 8 Soil state following lateral loading, at 0.04 mudline displacement (D_R = 38%), void ratio, e (LHS), horizontal stress (kPa), σ_{11} (RHS).

Figure 9 Soil state changes following lateral loading, at 0.04 mudline displacement (D_R = 38%), changes in void ratio, Δe (LHS), changes in horizontal stress (kPa), $\Delta\sigma_{11}$ (RHS).

Figure 10 p-y curve generated from numerical analysis results, D_R = 38%.

Figure 11 Normalised load-displacement curve for different initial relative density (5.22 m pile)

Figure 12 Normalised secant stiffness for different initial relative densities (5.22 m pile)

Figure 13 Effect of driving distance on the lateral capacity and stiffness (5.22 m pile)

Figure 14 Normalised load-displacement curve for 5.22 m and 8 m pile, wished-in-place piles

Figure 15 Normalised load-displacement curves for 5.22 m and 8 m pile, different installation methods

Figure 16 Normalised load-displacement curve for different initial relative density (8 m pile)

Figure 17 Effect of load eccentricity following different installation methods (8 m pile)

FIGURE

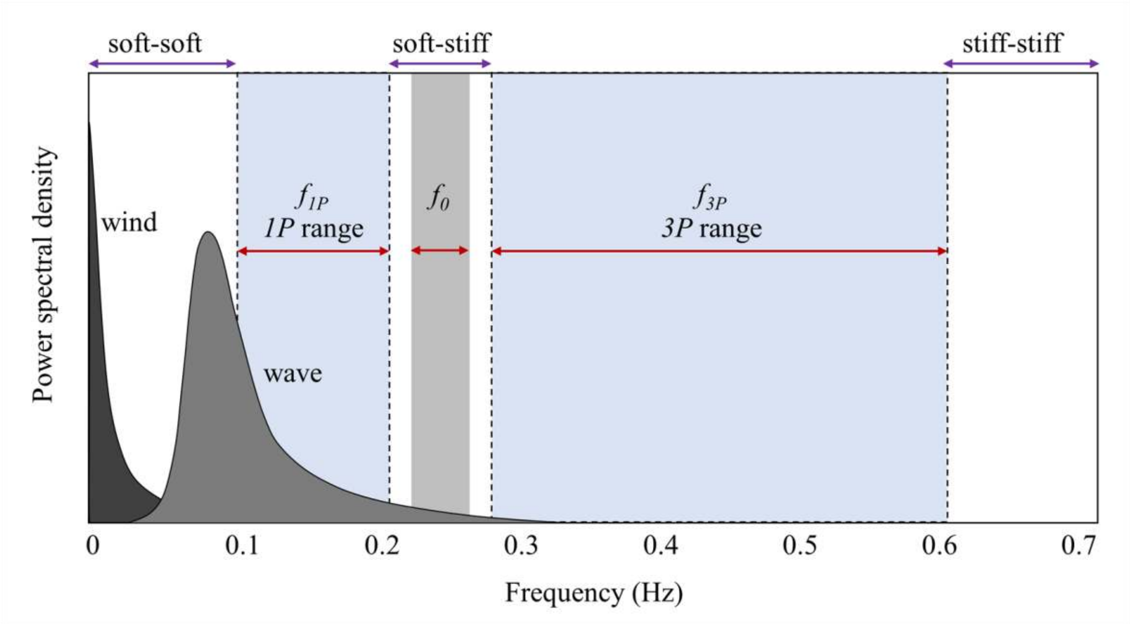

Figure 1 Excitation ranges of OWTs in the frequency domain (after Kallehave et al., 2015)

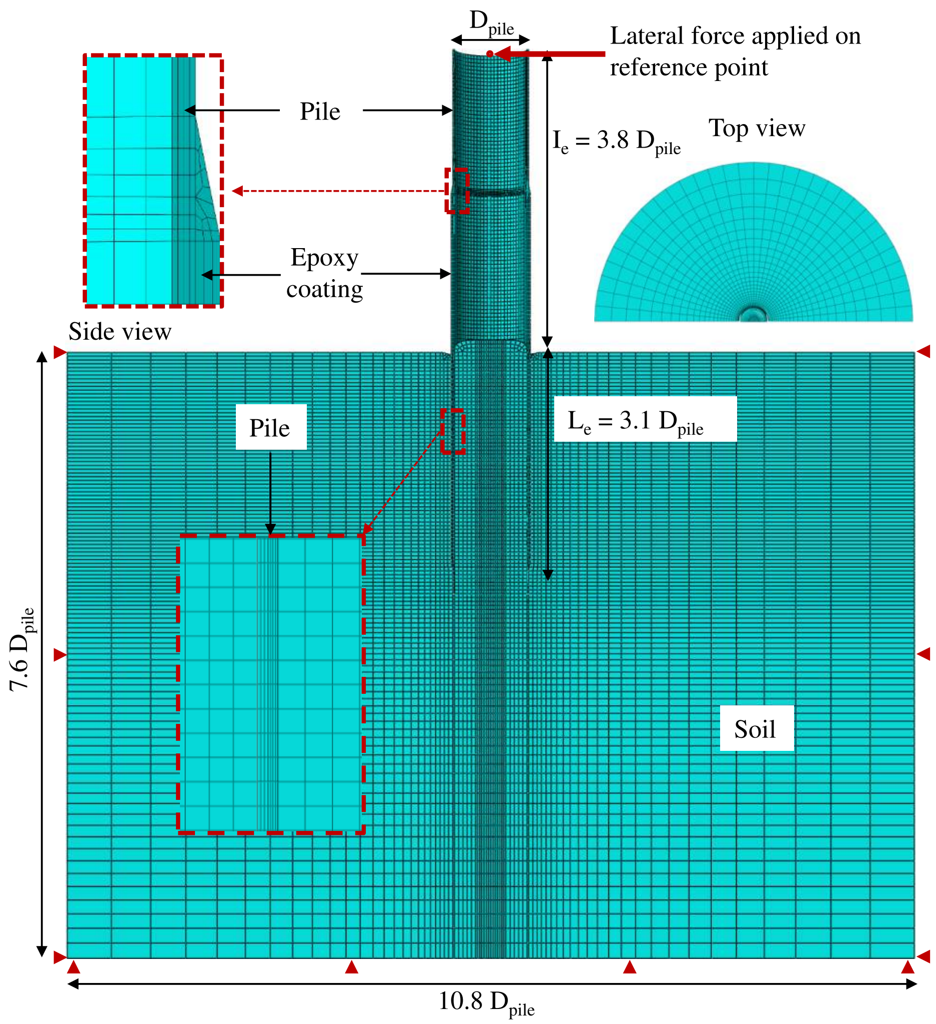

Figure 2 Lateral loading model (mesh, boundary conditions)

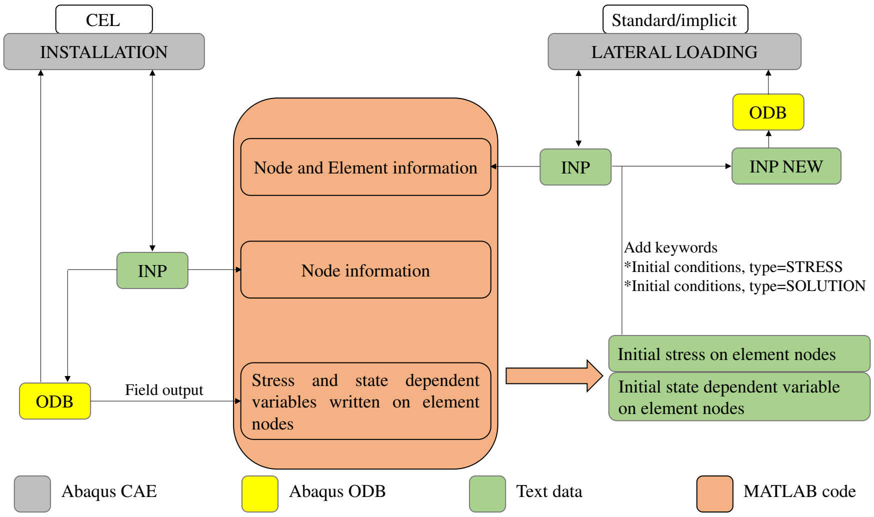

655

656 Figure 3 Mapping procedure from pile installation model to lateral loading model

657

a)

b)

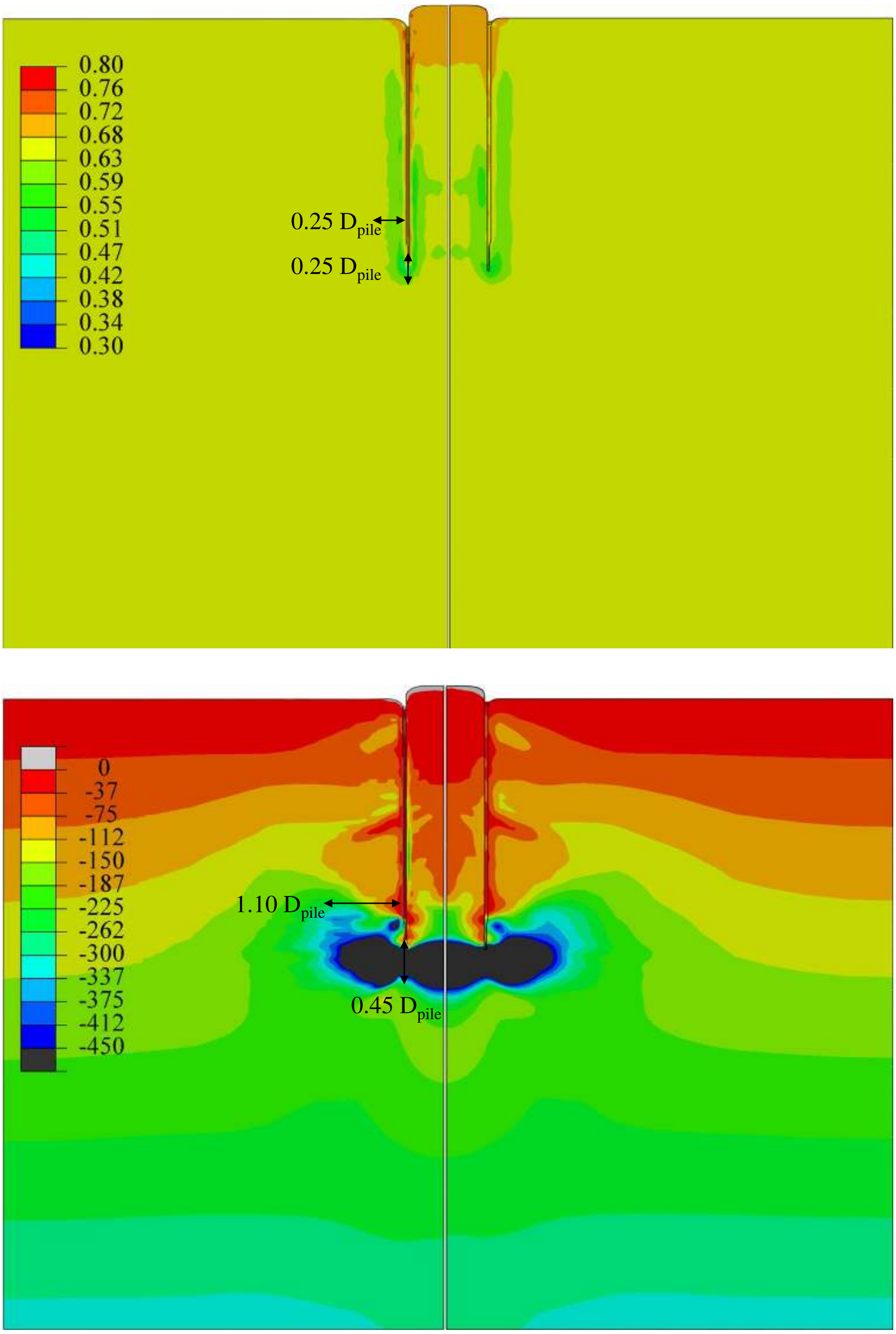

Figure 4 Soil state following jacked pile installation (D_R = 38%), (a) void ratio (b) horizontal stress (kPa). Results from pile installation (LHS, Fan et al. 2020) and mapped to pile lateral loading model (RHS)

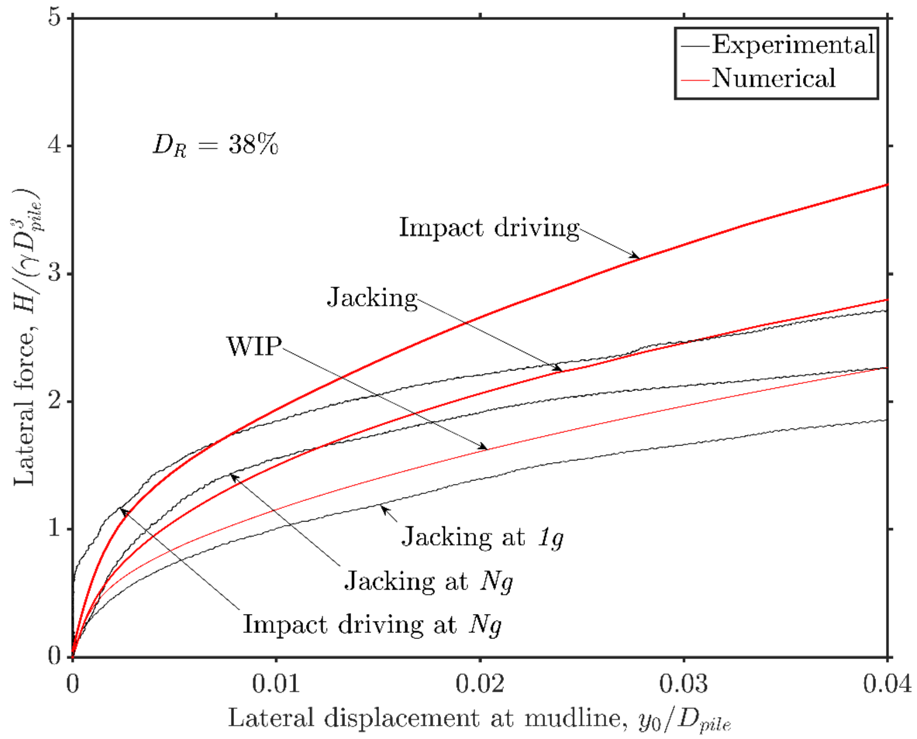

Figure 5 Comparison of normalised load-displacement curves between current numerical study and centrifuge test data, D_R = 38%

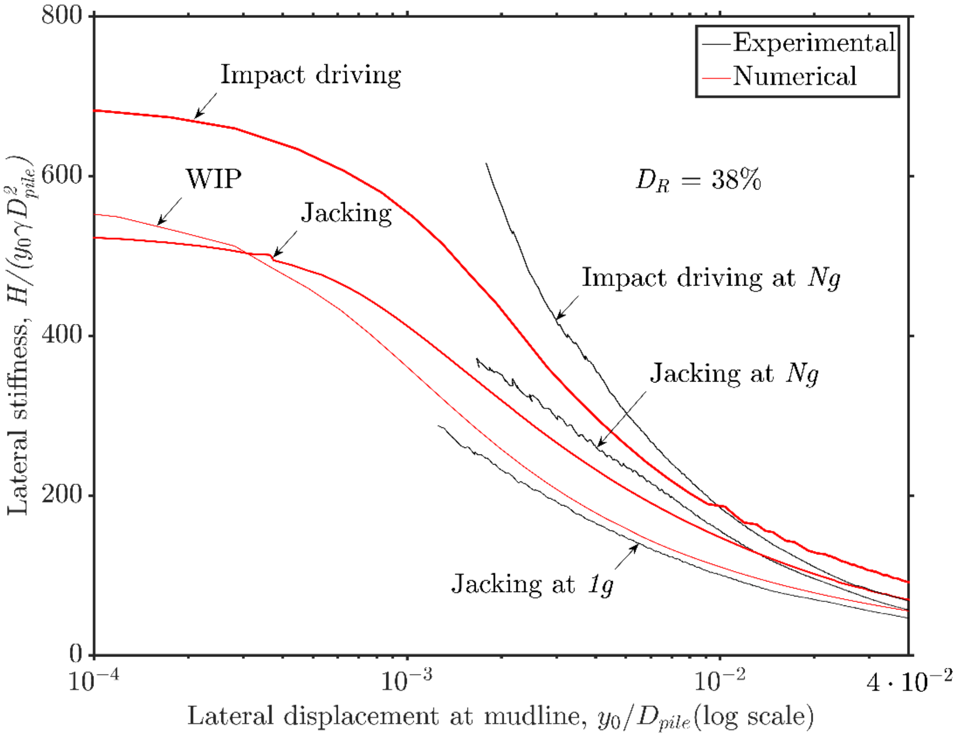

Figure 6 Comparison of normalised secant stiffness between current numerical study and centrifuge test, D_R = 38%

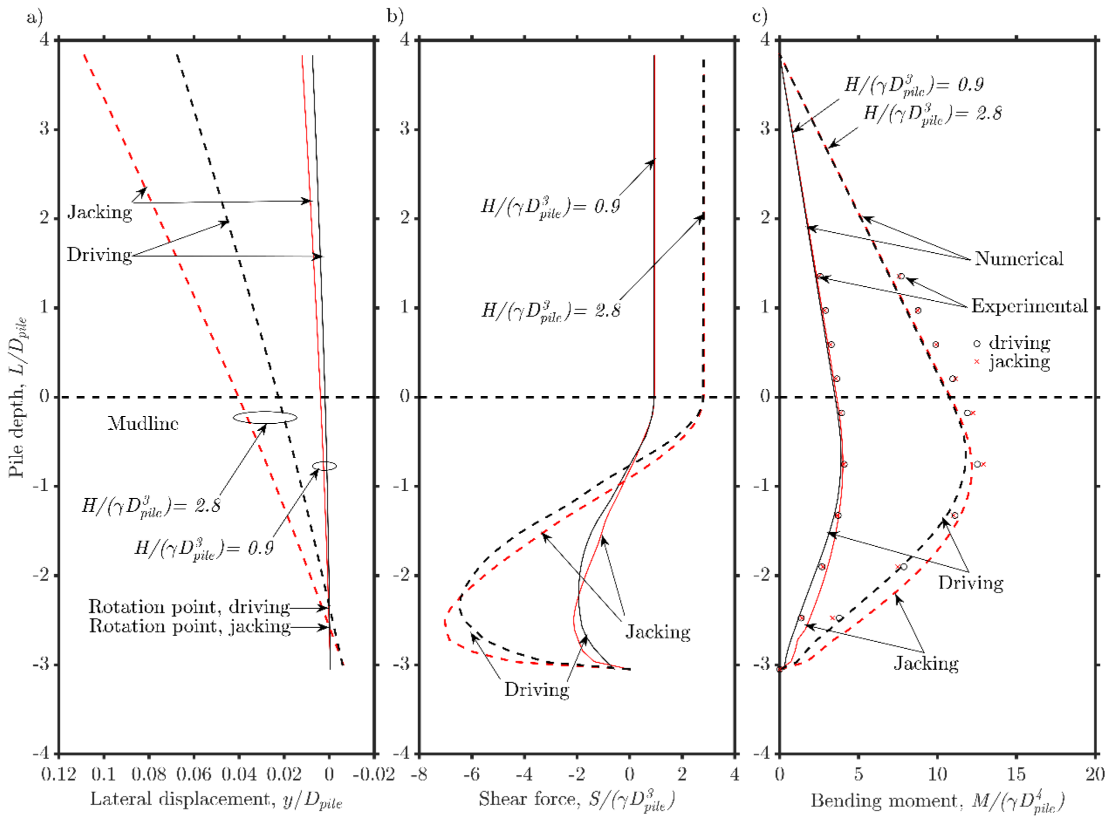

Figure 7 Deflection, shear force, and bending moment profiles along the entire pile length

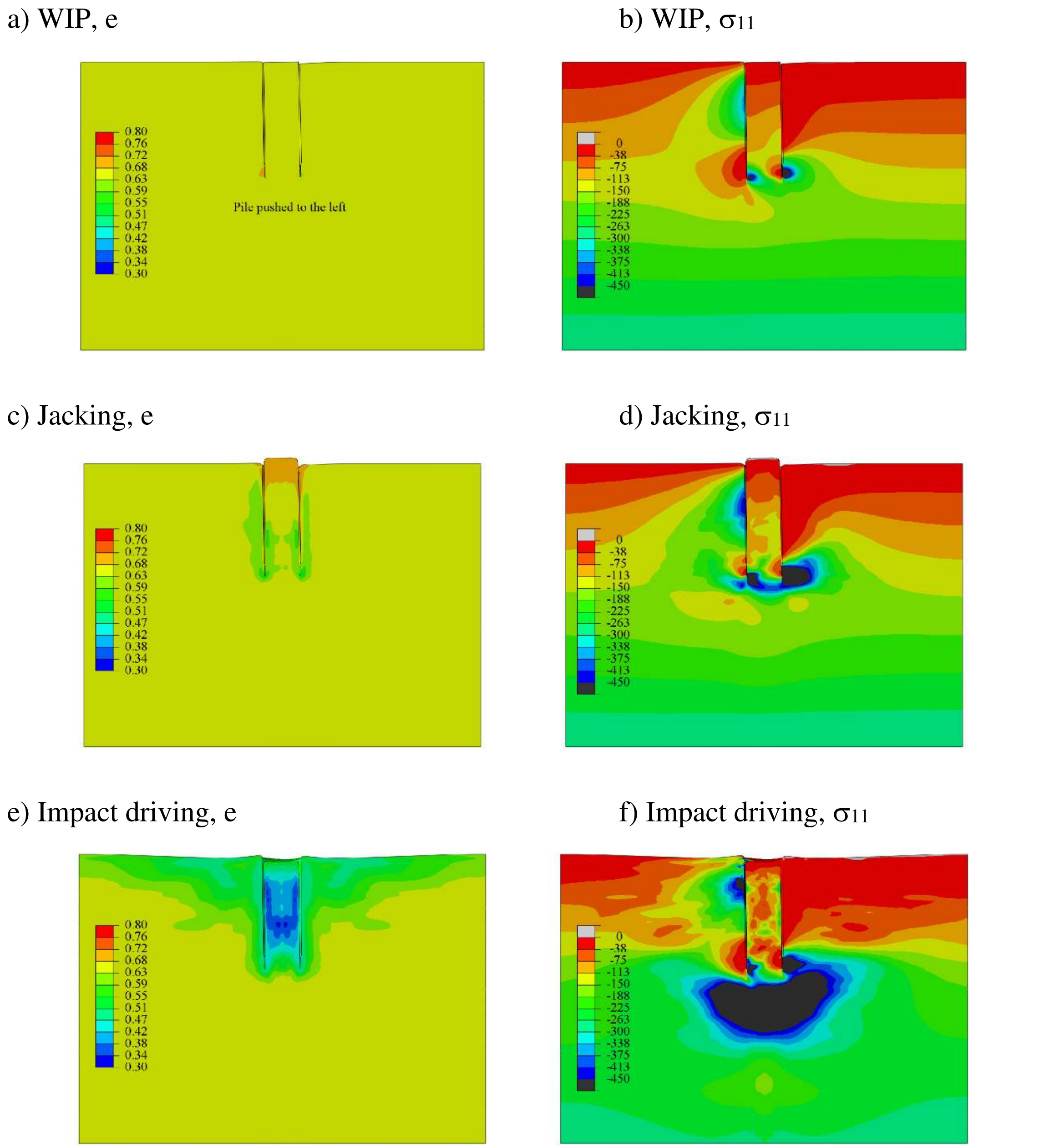

Figure 8 Soil state following lateral loading, at 0.04 mudline displacement (D_R = 38%), void ratio, e (LHS), horizontal stress (kPa), σ_{11} (RHS).

a) WIP, Δe

b) WIP, $\Delta\sigma_{11}$

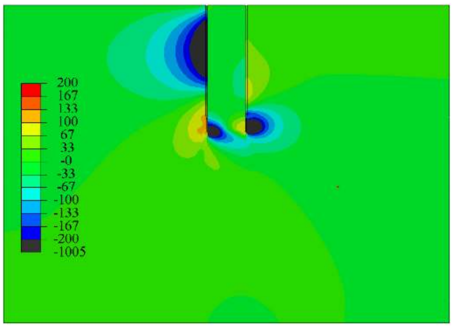

c) Jacking, Δe

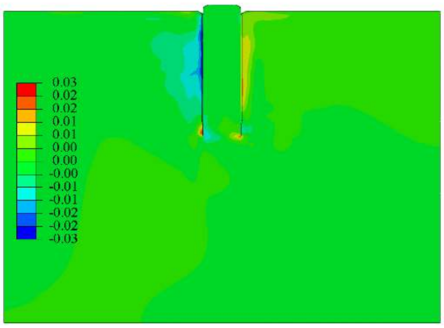

d) Jacking, $\Delta\sigma_{11}$

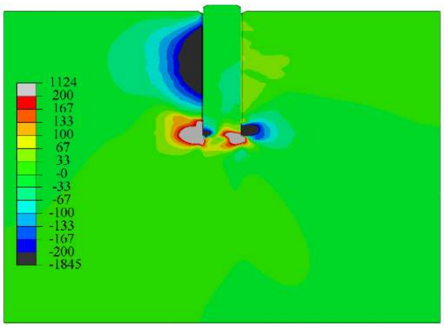

e) Impact driving, Δe

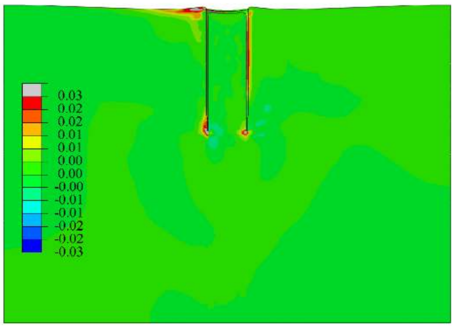

f) Impact driving, $\Delta\sigma_{11}$

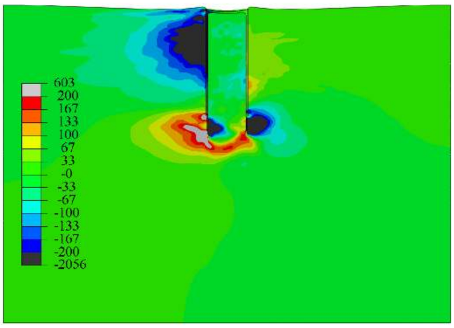

Figure 9 Soil state changes following lateral loading, at 0.04 mudline displacement (D_R = 38%), changes in void ratio, Δe (LHS), changes in horizontal stress (kPa), $\Delta\sigma_{11}$ (RHS).

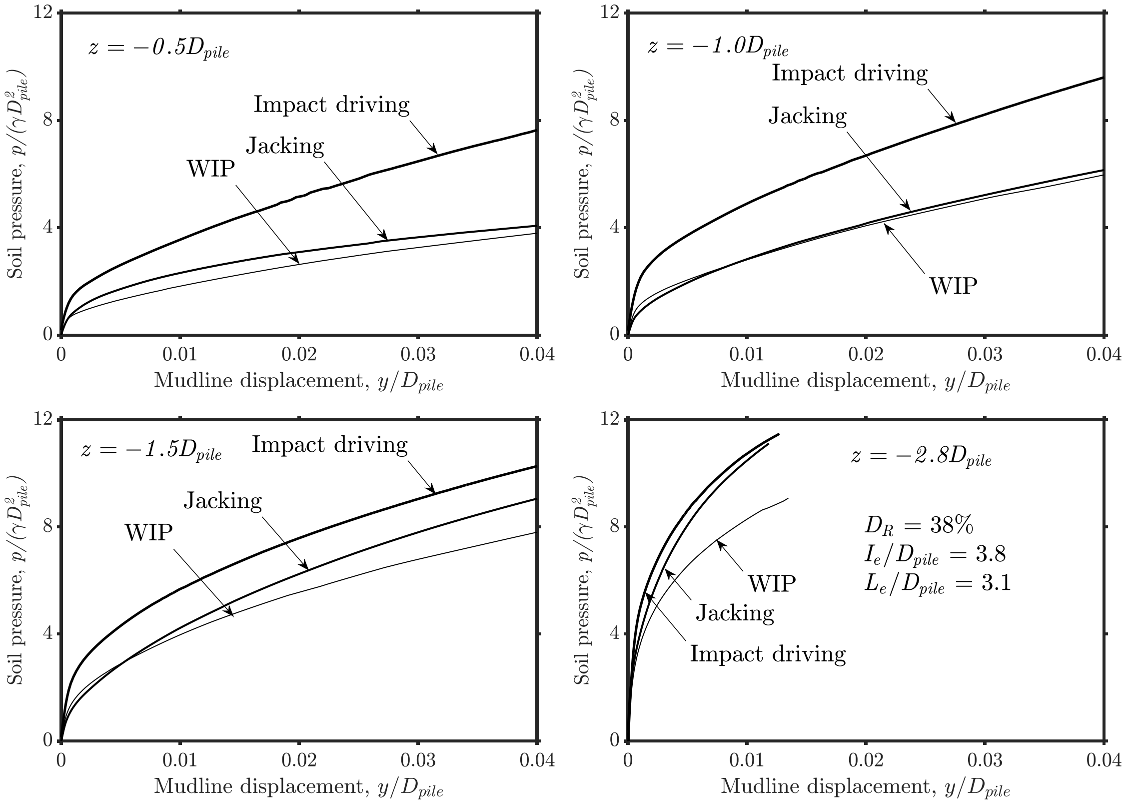

Figure 10 p-y curve generated from numerical analysis results, D_R = 38%.

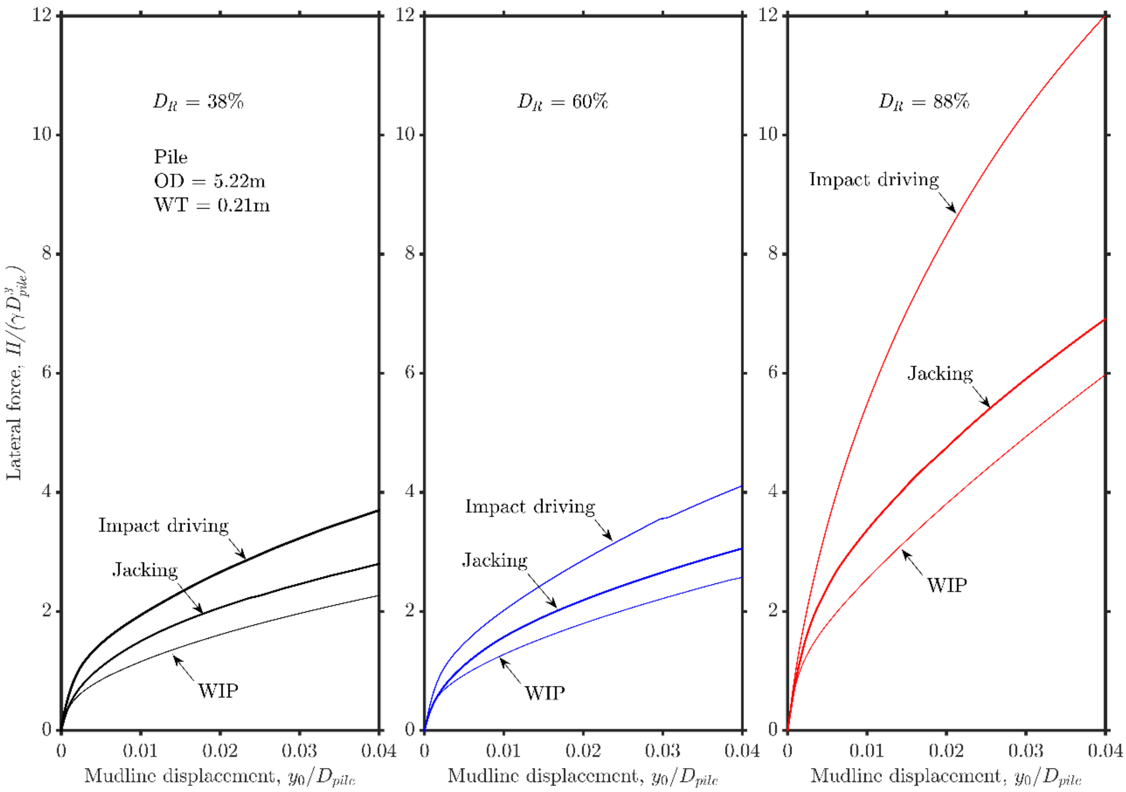

Figure 11 Normalised load-displacement curve for different initial relative density (5.22 m pile)

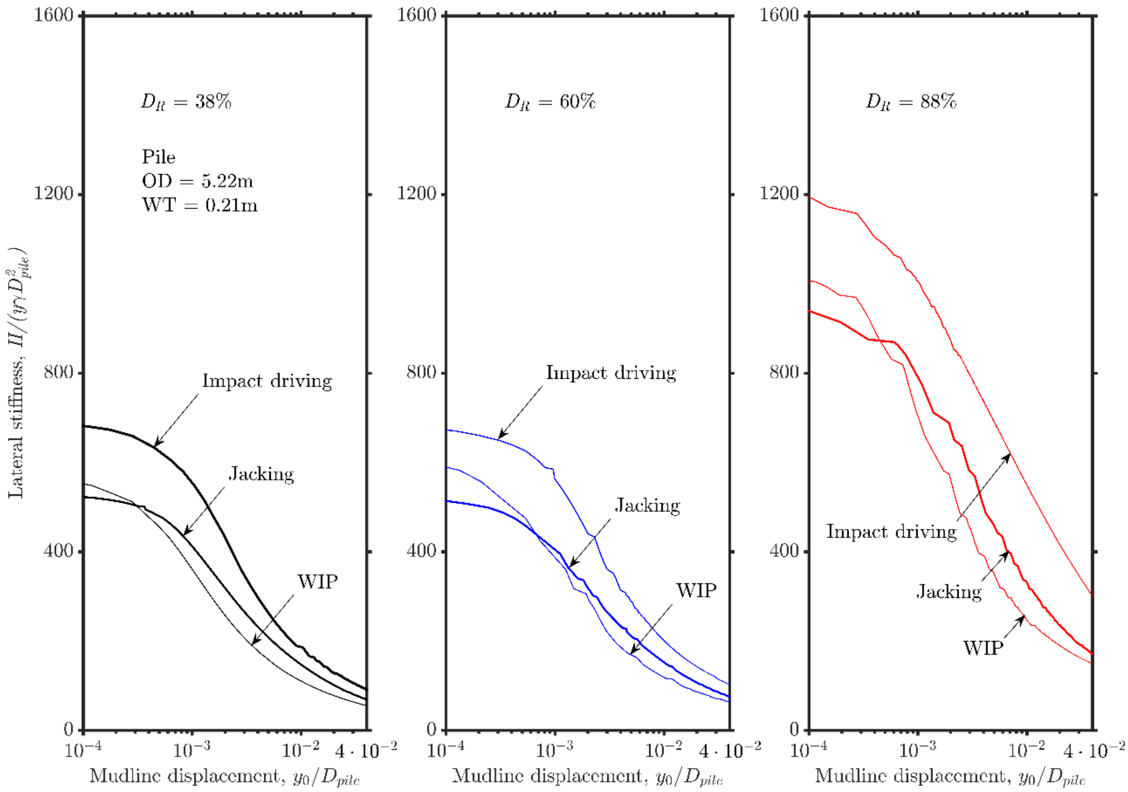

Figure 12 Normalised secant stiffness for different initial relative densities (5.22 m pile)

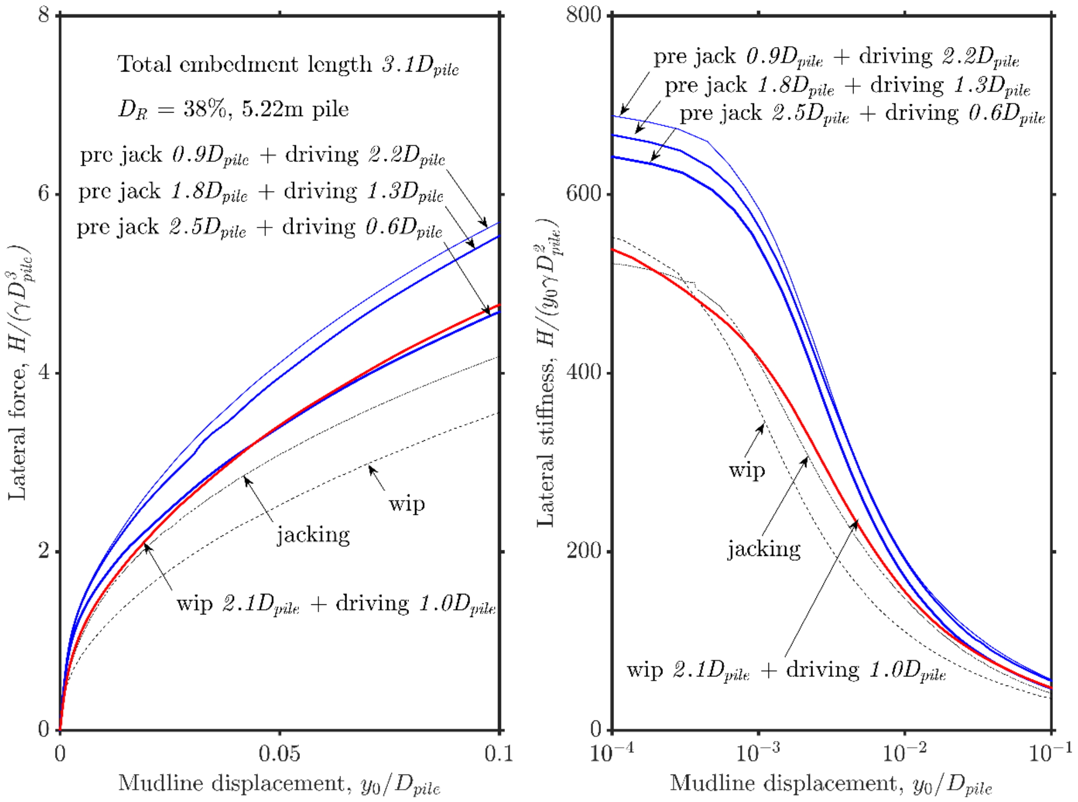

Figure 13 Effect of driving distance on the lateral capacity and stiffness (5.22 m pile)

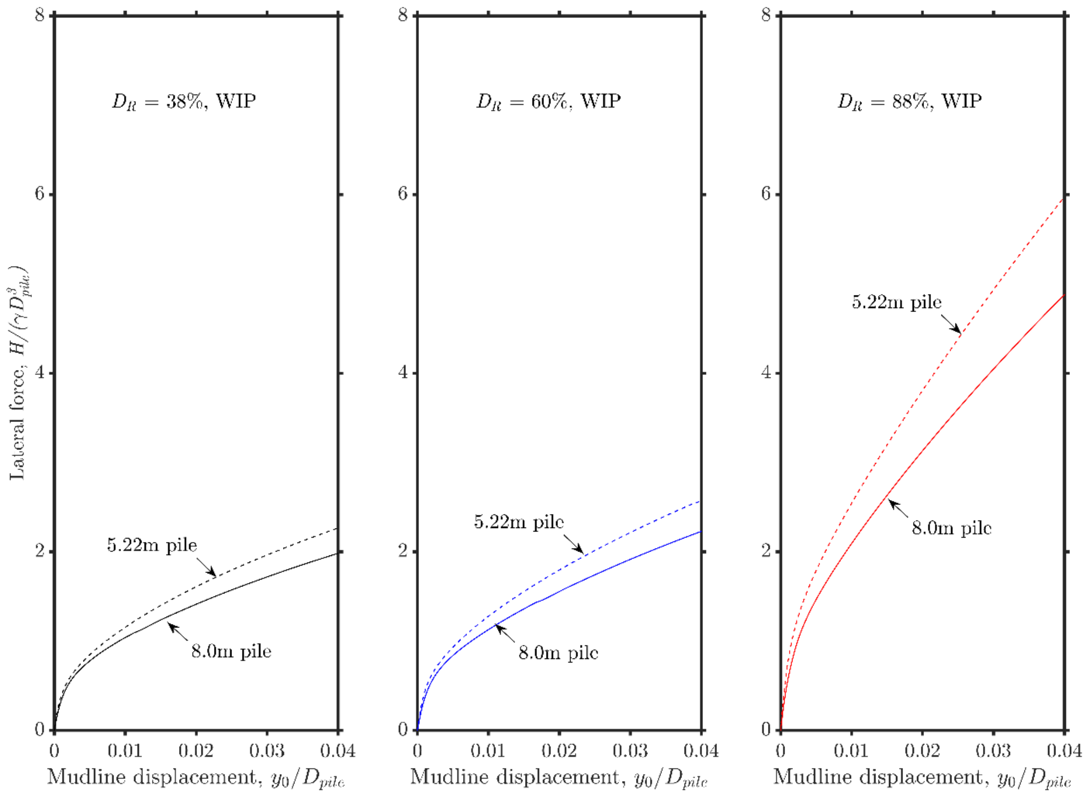

Figure 14 Normalised load-displacement curve for 5.22 m and 8 m pile, wished-in-place piles

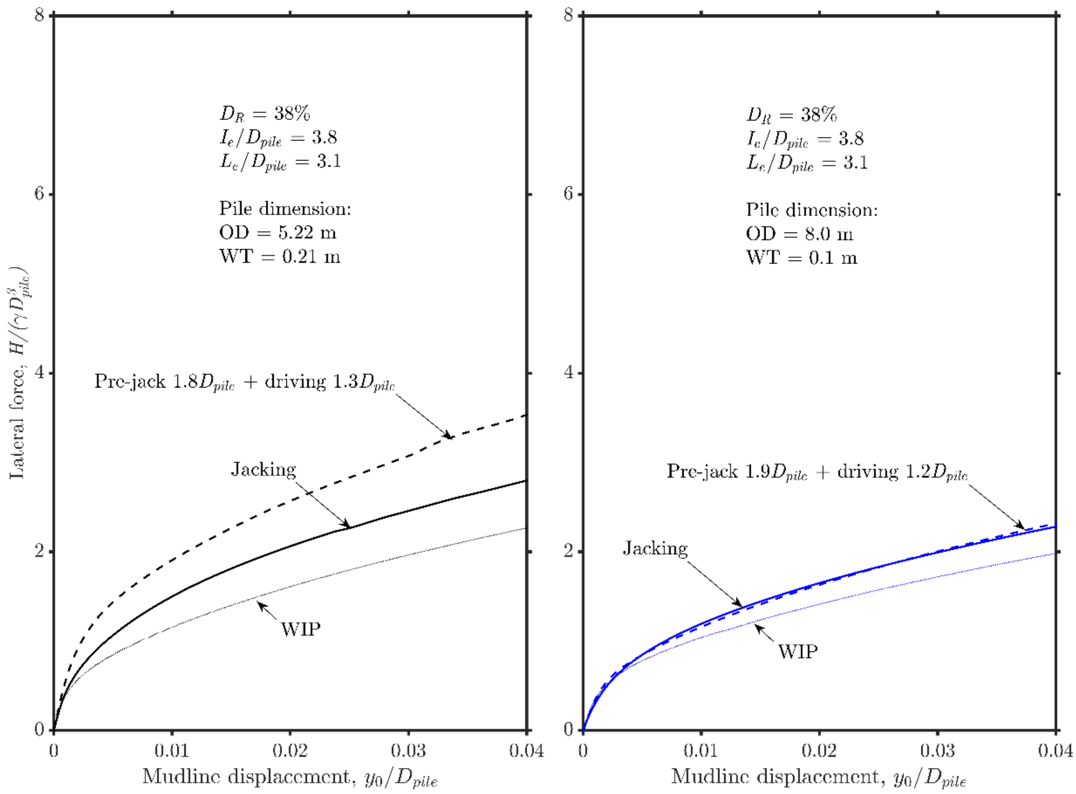

Figure 15 Normalised load-displacement curves for 5.22 m and 8 m pile, different installation methods

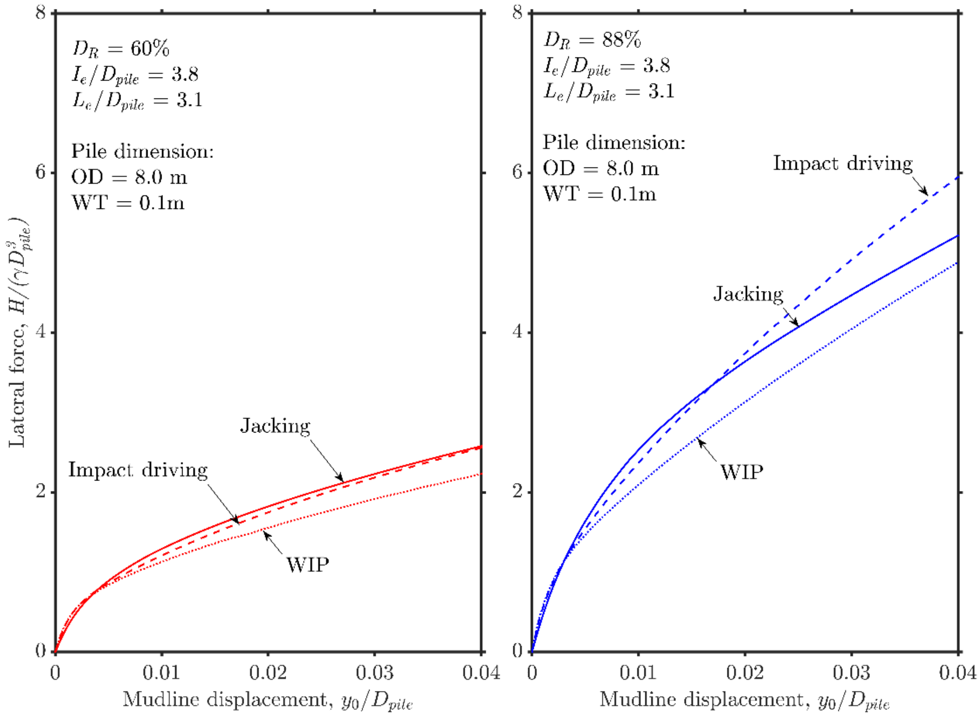

Figure 16 Normalised load-displacement curve for different initial relative density (8 m pile)

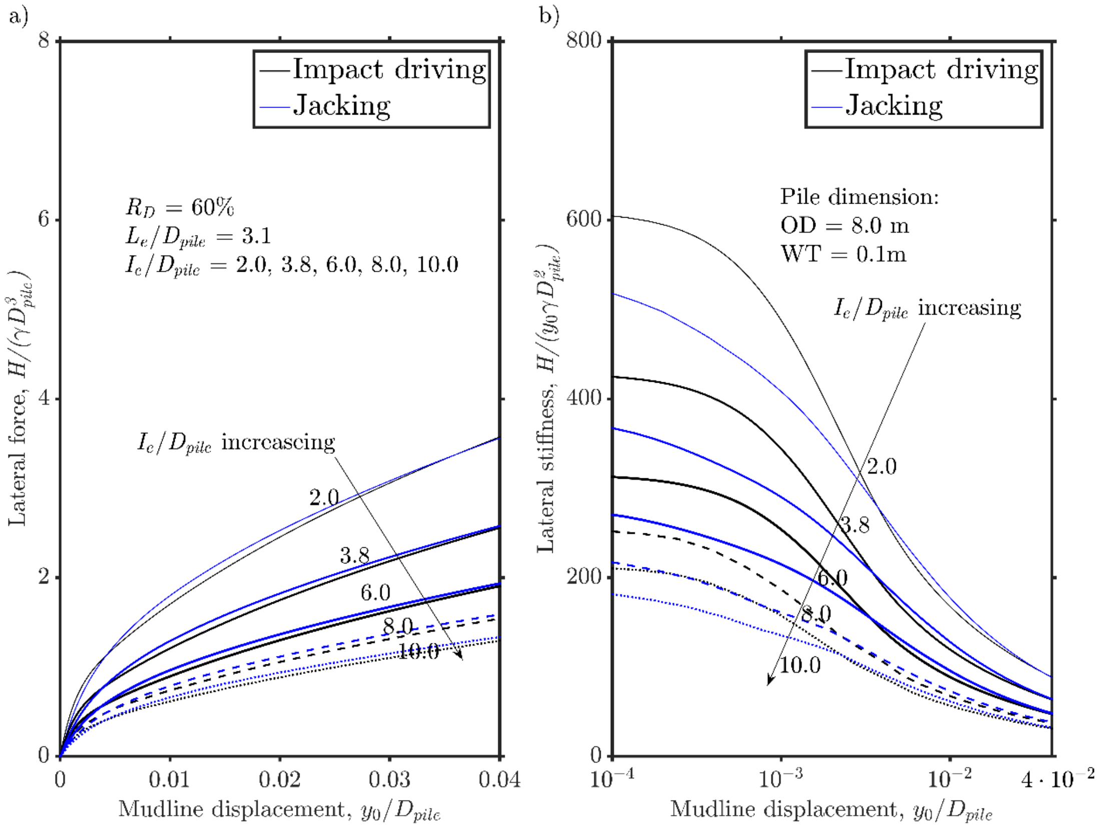

Figure 17 Effect of load eccentricity following different installation methods (8 m pile)